Calculation of Three-Dimensional Boundary Layers II. Three-Dimensional Flows in Cartesian Coordinates

Tuncer Cebeci*
Douglas Aircraft Company, Long Beach, Calif.

This paper presents a general method for solving the laminar and turbulent boundary-layer equations for three-dimensional flows in Cartesian coordinates. In the equations the Reynolds shear-stress terms appearing in the momentum equations for turbulent flows are modeled by an eddy-viscosity formulation developed by the author. The governing equations are solved by a very efficient two-point finite-difference method. The accuracy of the method is investigated for both laminar and turbulent flows.

Nomenclature

A = Van Driest damping parameter
f = similarity variable for ψ
g = similarity variable for ϕ
J = total number of grid points in η-direction
K = variable grid parameter
L = modified mixing length, Eq. (12a)
N = dimensionless parameter, Eq. (12c)
p = pressure
p^+ = dimensionless pressure-gradient parameter, Eq. (12d)
u,v,w = velocity components in the x,y,z-directions, respectively
v_w^+ = dimensionless mass transfer parameter, Eq. (12d)
u_τ = friction velocity, Eq. (12b)
u_t = total velocity, Eq. (12d)
w_z = derivative of w with respect to z, $\partial w/\partial z$
x,y,z = Cartesian coordinates
δ = boundary-layer thickness
ϵ = eddy viscosity
ϵ^+ = dimensionless eddy viscosity, ϵ/ν
η = similarity variable for y
η_∞ = transformed boundary-layer thickness
μ = dynamic viscosity
ν = kinematic viscosity
ρ = density
$\phi\ \psi$ = components of vector potential

Subscripts

e = outer edge of boundary layer
w = wall
∞ = freestream conditions

Primes denote differentiation with respect to η

I. Introduction

In recent years, several accurate methods have been developed to compute three-dimensional boundary layers. For example, in Ref. 1, Hunt et al., developed a finite-difference method for analyzing compressible turbulent boundary layers on a blunt swept slab with leading edge blowing. In that reference, the Reynolds shear stress terms were modeled by using a mixing-length expression which was based on a generalization of the two-dimensional model used earlier by Bushnell and Beckwith.[2] That model has been adopted by Adams and was used to compute several semi-three dimensional turbulent boundary layers.[3] In Ref. 4, Bradshaw extended his two-dimensional method to compute three-dimensional flows past infinite swept wings and obtained good agreement with experiment. His method differs from the previously mentioned ones in that his modeling of the Reynolds shear-stress terms does not use the mixing-length concepts; rather it uses the turbulence kinetic energy equation, a model that has been used extensively by Nash.[5] Recently Harris and Morris[6] developed an accurate and efficient method to compute full three-dimensional compressible laminar and turbulent boundary layers. Their method uses an eddy viscosity method and gives results that agree well with experiment.

In this paper we present a very efficient method to calculate three-dimensional incompressible laminar and turbulent boundary layers in Cartesian coordinates. The method uses an eddy-viscosity formulation to model the Reynolds shear-stress terms and a very efficient numerical method to solve the governing equations. The model has previously been used to compute three-dimensional boundary layers on infinite swept cylinders and three-dimensional boundary layers with small crossflow.[7] The accuracy of the method was thoroughly studied with the available experimental data and with the results obtained by Bradshaw's method. The study showed that the predictions of the method were in good agreement with both.

In Sec. II and III we present the governing equations and the eddy-viscosity formulas for three-dimensional laminar and turbulent boundary layers. When physical coordinates are used, the solutions of the governing boundary-layer equations are quite sensitive to the spacings in the streamwise (x), and the crosswise direction (z), and require a large number of x- and z-stations. In problems where computation time and storage become important, it is necessary to remove the sensitivity to Δx- and Δz-spacings. That can be done by expressing and by solving the governing equations in transformed coordinates. We, therefore, consider in Sec. IV, a convenient transformation and express the boundary-layer equations in terms of transformed variables.

In Sec. V we discuss the numerical method, and in Sec. VI we discuss the results obtained by the present method for both laminar and turbulent flows.

In our studies we observe that the present method is quite accurate and suitable for solving three-dimensional flows in Cartesian coordinates. The computation time is very small. A turbulent flow consisting of 30 streamwise stations, 4 crosswise stations, and 20-30 grid points across the boundary layer can be solved in 0.201 min of CPU (Central-Processing-Unit)-time on an IBM 370/165. A laminar flow consisting of 30 streamwise stations, 15 crosswise stations with 30 points across the boundary layer can be solved in 0.486 min of CPU-time.

Received July 31, 1974; revision received February 6, 1975. This work was supported by the Naval Ship Research and Development Center under Contract N00014-72-C-0111, Subsonic SR 009 01-01.

Index category: Boundary Layers and Convective Heat Transfer, Turbulent.

*Chief Aerodynamics Engineer for Research. Member AIAA.

II. The Boundary-Layer Equations in Cartesian Coordinates

The governing boundary-layer equations for three-dimensional incompressible flows in Cartesian coordinate system are given by the following equations

Continuity

$$(\partial u/\partial x) + (\partial w/\partial z) + (\partial v/\partial y) = 0 \tag{1}$$

x-Momentum

$$u\frac{\partial u}{\partial x} + w\frac{\partial u}{\partial z} + v\frac{\partial u}{\partial y} = -\frac{1}{\rho}\frac{\partial p}{\partial x} + \frac{1}{\rho}\frac{\partial}{\partial y}\left(\mu\frac{\partial u}{\partial y} - \rho\overline{u'v'}\right) \tag{2}$$

z-Momentum

$$u\frac{\partial w}{\partial x} + w\frac{\partial w}{\partial z} + v\frac{\partial w}{\partial y} = -\frac{1}{\rho}\frac{\partial p}{\partial z} + \frac{1}{\rho}\frac{\partial}{\partial y}\left(\mu\frac{\partial w}{\partial y} - \rho\overline{w'v'}\right) \tag{3}$$

At the edge of the boundary layer, Eqs. (2) and (3) reduce to

$$u_e\frac{\partial u_e}{\partial x} + w_e\frac{\partial u_e}{\partial z} = -\frac{1}{\rho}\frac{\partial p}{\partial x} \tag{4a}$$

$$u_e\frac{\partial w_e}{\partial x} + w_e\frac{\partial w_e}{\partial z} = -\frac{1}{\rho}\frac{\partial p}{\partial z} \tag{4b}$$

The boundary conditions for Eqs. (1)-(3) for zero mass transfer are

$$y=0, \quad u,w=0, \quad v=0 \tag{5a}$$

$$y=\delta, \quad u=u_e(x,z), \quad w=w_e(x,z) \tag{5b}$$

The solution of the system given by Eqs. (1-5) requires closure assumptions for the Reynolds stresses appearing in these equations. They also require initial conditions on 2 intersecting planes. In some problems we can take advantage of the symmetry conditions and can obtain one of the initial conditions by noting that on the line of symmetry the flow is two-dimensional except for the cross-flow derivatives. The flow in that direction is usually referred to as the attachment-line flow, because the attachment line is a streamline on the body on which both the cross-flow velocity components in the boundary layer and the cross-flow pressure gradient are identically zero. Since w and $\partial p/\partial z$ are zero on the attachment line, the z-momentum equation is singular on that line. However, differentiation with respect to z will yield a non-singular equation. After performing the necessary differentiation for the z-momentum equation and taking advantage of symmetry conditions ($\partial u/\partial z = \partial v/\partial z = \partial^2 w/\partial z^2 = 0$) we can write the governing *attachment-line flow equations* as

Continuity:

$$(\partial u/\partial x) + w_z + (\partial v/\partial y) = 0 \tag{6}$$

x-Momentum

$$u\frac{\partial u}{\partial x} + v\frac{\partial u}{\partial y} = u_e\frac{\partial u_e}{\partial x} + \frac{1}{\rho}\frac{\partial}{\partial y}\left(\mu\frac{\partial u}{\partial y} - \rho\overline{u'v'}\right) \tag{7}$$

z-Momentum

$$u\frac{\partial w_z}{\partial x} + v\frac{\partial w_z}{\partial y} + w_z^2 = u_e\frac{\partial}{\partial x}(w_z)_e + (w_z)_e^2 + \frac{1}{\rho}\frac{\partial}{\partial y}\left[\mu\frac{\partial w_z}{\partial y} - \rho(\overline{w'v'})_z\right] \tag{8}$$

where $w_z = \partial w/\partial z$.

These equations are subject to the following boundary conditions

$$y=0, \quad u, w_z = 0, \quad v=0 \tag{9a}$$

$$y=\delta, \quad u=u_e(x,z), \quad w_z = w_{ze} \tag{9b}$$

III. Closure Assumptions for the Reynolds Shear Stresses

Equations (1-5) or (6-9) form a highly coupled system which is difficult to solve. In addition, they contain the Reynolds shear stress terms for which a closure assumption must be made. In the study reported here we satisfy the closure assumptions by using the eddy-viscosity concept and relate the Reynolds shear stresses to the mean velocity profiles by

$$-\rho\overline{u'v'} = \rho\epsilon_1(\partial u/\partial y), \quad -\rho\overline{w'v'} = \rho\epsilon_2(\partial w/\partial y) \tag{10}$$

As in Ref. 7, we assume that $\epsilon_1 = \epsilon_2 = \epsilon$ and define ϵ by two separate formulas. In the so-called inner region of the boundary layer ϵ is defined by the following formula

$$\epsilon_i = L^2[(\partial u/\partial y)^2 + (\partial w/\partial y)^2]^{1/2} \tag{11}$$

where

$$L = 0.4y[1 - \exp(-y/A)] \tag{12a}$$

$$A = 26\frac{\nu}{N}u_\tau^{-1}, \quad u_\tau = \left(\frac{\tau_t}{\rho}\right)^{1/2},$$

$$\frac{\tau_t}{\rho} = \nu[(\partial u/\partial y)_w^2 + (\partial w/\partial y)_w^2]^{1/2} \tag{12b}$$

$$N = \left[(p^+/v_w^+)[1 - \exp(11.8v_w^+)] + \exp(11.8v_w^+)\right]^{1/2} \tag{12c}$$

$$v_w^+ = (v_w/u_\tau), \quad p^+ = (\nu u_t/u_\tau^3)(\mathrm{d}u_t/\mathrm{d}s),$$

$$u_t = (u_e^2 + w_e^2)^{1/2} \tag{12d}$$

$$\frac{\mathrm{d}}{\mathrm{d}s} = \frac{\partial}{\partial x}\frac{\mathrm{d}x}{\mathrm{d}s} + \frac{\partial}{\partial z}\frac{\mathrm{d}z}{\mathrm{d}s} = \frac{u_e}{u_t}\frac{\partial}{\partial x} + \frac{w_e}{u_t}\frac{\partial}{\partial z} \tag{12e}$$

In the outer region ϵ is defined by the following formula

$$\epsilon_0 = 0.0168\left[\int_0^\infty [u_t - (u^2+w^2)^{1/2}]\,\mathrm{d}y\right] \tag{13}$$

IV. Transformation of the Governing Equations

The boundary-layer equations (1-3) can be solved when they are expressed either in physical coordinates or in transformed coordinates. Each coordinate has its own advantages. In problems where the computer storage becomes important, the choice of using transformed coordinates becomes necessary, as well as convenient, since the transformed coordinates allow

large steps to be taken in the x and z directions. The reason is that the profiles expressed in the transformed coordinates do not change as rapidly as they do when they are expressed in physical coordinates. The use of transformed coordinates stretches the coordinate normal to the flow and takes out much of the variation in boundary-layer thickness for laminar flows. In addition, they remove the singularity that the equations in physical coordinates have at $x=0$ and $z=0$.

We first define the transformed coordinates by

$$x=x, \qquad z=z, \qquad \eta=(u_e/\nu x)^{1/2}y \tag{14}$$

and introduce a two-component vector potential such that

$$u=(\partial\psi/\partial y), \quad w=(\partial\phi/\partial y), \quad v=-\left(\frac{\partial\psi}{\partial x}+\frac{\partial\phi}{\partial z}\right) \tag{15}$$

In addition, we define dimensionless ψ and ϕ by

$$\psi=(u_e\nu x)^{1/2}f(x,z,\eta) \tag{16a}$$

$$\phi=(\nu x/u_e)^{1/2}w_e g(x,z,\eta) \tag{16b}$$

Using these transformations and using Eq. (10) to replace the Reynolds shear stress terms in the momentum equations, after some rearranging, we get

x-Momentum

$$[(1+\epsilon^+)f'']'+P_1 ff''+P_2[1-(f')^2]+P_5(1-f'g')+P_6 gf''=x\left[f'\frac{\partial f'}{\partial x}-f''\frac{\partial f}{\partial x}+\frac{w_e}{u_e}\left[g'\frac{\partial f'}{\partial z}-f''\frac{\partial g}{\partial z}\right]\right] \tag{17}$$

z-Momentum

$$[(1+\epsilon^+)g'']'+P_2 fg''+P_4(1-f'g')+P_3[1-(g')^2]+P_6 gg''=x\left[f'\frac{\partial g'}{\partial x}-g''\frac{\partial f}{\partial x}+\frac{w_e}{u_e}\left[g'\frac{\partial g'}{\partial z}-g''\frac{\partial g}{\partial z}\right]\right] \tag{18}$$

Here

$$f'=u/u_e, \qquad g'=w/w_e,$$

$$P_2=\frac{x}{u_e}\frac{\partial u_e}{\partial x}, \quad P_1=\frac{P_2+1}{2}, \quad P_3=\frac{x}{u_e}\frac{\partial w_e}{\partial z},$$

$$P_4=\frac{x}{w_e}\frac{\partial w_e}{\partial x}, \quad P_5=\frac{w_e}{u_e}\frac{x}{u_e}\frac{\partial u_e}{\partial z}, \quad P_6=P_3-\frac{P_5}{2} \tag{19a}$$

The boundary conditions (5) become

$$\eta=0, \quad f=g=0, \quad f'=g'=0 \tag{19b}$$

$$\eta=\eta_\infty \quad f'=g'=1 \tag{19c}$$

The attachment-line equations can also be transformed by a similar procedure. This time, we define the two-component vector potential by

$$u=(\partial\psi/\partial y), \quad w_z=(\partial\phi/\partial y), \quad v=-(\partial\psi/\partial x+\phi) \tag{20}$$

and again use the expressions given by Eq. (16) except that now we define ϕ by

$$\phi(\nu x/u_e)^{1/2}\, w_{ze}g(x,z,\eta) \tag{21}$$

Introducing the expressions (14, 16a, 20, and 21) into Eqs. (7) and (8), we get

x-Momentum

$$[(1+\epsilon^+)f'']'+P_1 ff''+P_2[1-(f')^2]+P_3 gf''=x\left[f'\frac{\partial f'}{\partial x}-f''\frac{\partial f}{\partial x}\right] \tag{22}$$

z-Momentum

$$[(1+\epsilon^+)g'']'+P_1 fg''+P_4(1-f'g')+P_3[1-(g')^2]+P_3 gg''=x\left[f'\frac{\partial g'}{\partial x}-g''\frac{\partial f}{\partial x}\right] \tag{23}$$

Here the definitions of the terms are the same as before except for g' and P_4,

$$g'=w_z/w_{ze}, \quad P_4=-\frac{x}{w_{ze}}\frac{\partial w_{ze}}{\partial x} \tag{24}$$

The boundary conditions (9) become

$$\eta=0, \quad f=g=0, \quad f'=g'=0 \tag{25a}$$

$$\eta=\eta_\infty, \quad f'=g'=1 \tag{25b}$$

V. Numerical Method

We use a very efficient two-point finite-difference method to solve the system given by Eqs. (17-19) and the system (22, 23, 25). This method was developed by H. B. Keller.[8] and has successfully been applied to the two-dimensional boundary-layer equations by Keller and Cebeci[9,10] and to the swept infinite cylinders and small cross flow by Cebeci.[7] Here we apply the method to full three-dimensional laminar and turbulent boundary layers. A detailed description of the method is presented in Refs. 10 and 11; for this reason only a brief description of it will be presented here.

We first consider the attachment-line Eqs. (22) and (23), and write them in terms of a first-order system of partial-differential equations. For this purpose we introduce new dependent variables $u(x,\eta)$, $v(x,\eta)$, $w(x,\eta)$, and $t(x,\eta)$ so that Eqs. (22) and (23) can be written as

$$f'=u \tag{26a}$$

$$u'=v \tag{26b}$$

$$g'=w \tag{26c}$$

$$w'=t \tag{26d}$$

$$(bv)'+P_1 fv+P_2(1-u^2)+P_3 gv=x\left[u\frac{\partial u}{\partial x}-v\frac{\partial f}{\partial x}\right] \tag{26e}$$

$$(bt)'+P_1 ft+P_4(1-uw)+P_3(1-w^2)+P_3 gt=x\left[u\frac{\partial w}{\partial x}-t\frac{\partial f}{\partial x}\right] \tag{26f}$$

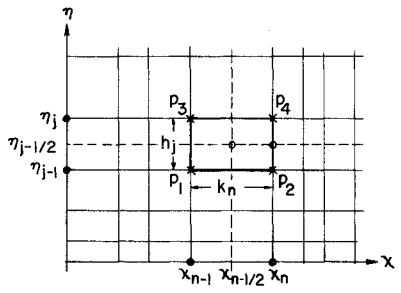

Fig. 1 Net rectangle for the difference equations for two-dimensional flows.

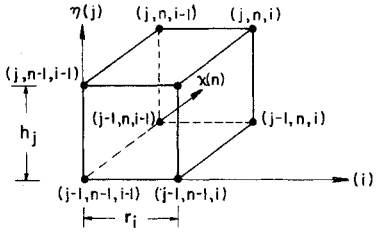

Fig. 2 Net cube for the difference equations for three-dimensional flows.

We next consider the net rectangle shown in Fig. 1. We denote the net points by

$$x_0=0, \quad x_n=x_{n-1}+k_n, \qquad n=1,2,\ldots, N$$

$$\eta_0=0, \quad \eta_j=\eta_{j-1}+h_j, \qquad j=1,2,\ldots, J;\ \eta_j=\eta_\infty \tag{27}$$

The net spacings, k_n and h_j, are completely arbitrary, and indeed may have large variations in practical calculations. This is especially important in turbulent boundary-layer calculations which are characterized by large boundary-layer thicknesses. To get accuracy near the wall, small net spacing is required while large spacing can be used away from the wall.

We approximate the quantities (f,u,v,g,w,t) at points (x_n,η_j) of the net by net functions denoted by $(f_j^n, u_j^n, v_j^n, g_j^n, w_j^n, t_j^n)$. We also employ the notation, for points and quantities midway between net points and for *any* net function q_j^n

$$x_{n-1/2} \equiv \tfrac{1}{2}(x_n+x_{n-1}), \eta_{j-1/2} \equiv \tfrac{1}{2}(\eta_j+\eta_{j-1})$$

$$q_j^{n-1/2} \equiv \tfrac{1}{2}(q_j^n+q_j^{n-1}), q_{j-1/2}^n \equiv \tfrac{1}{2}(q_j^n+q_{j-1}^n) \tag{28}$$

The difference equations which are to approximate Eq. (26) are now easily formulated by considering one mesh rectangle as in Fig. 1. We approximate Eqs. (26a-c) using centered difference quotients and average about the midpoint $(x_n, \eta_{J-1/2})$ of the segment P_2P_4.

$$(f_j^n-f_{j-1}^n)/h_j=u_{j-1/2}^n \tag{29a}$$

$$(u_j^n-u_{j-1}^n)/h_j=v_{j-1/2}^n \tag{29b}$$

$$(g_j^n-g_{j-1}^n)/h_j=w_{j-1/2}^n \tag{29c}$$

$$(w_j^n-w_{j-1}^n)/h_j=t_{j-1/2}^n \tag{29d}$$

Similarly Eqs. (26e) and (26f) are approximated by centering about the midpoint $x_{n-1/2}$, $\eta_{j-1/2}$ of the rectangle $P_1P_2P_3P_4$. This gives

$$[((bv)_j^n-(bv)_{j-1}^n)/h_j]+(P_1^n+\alpha_n)\ (fv)_{j-1/2}^n$$
$$-(P_2^n+\alpha_n)\ (u^2)_{j-1/2}^n+P_3^n\ (gv)_{j-1/2}^n$$
$$+\alpha_n(f_{j-1/2}^n v_{j-1/2}^{n-1}-v_{j-1/2}^n f_{j-1/2}^{n-1})=T_{j-1/2}^{n-1} \tag{29e}$$

$$[((bt)_j^n-(bt)_{j-1}^n)/h_j]+P_1^n\ (ft)_{j-1/2}^n-(P_4^n+\alpha_n)\ (uw)_{j-1/2}^n$$
$$P_3^n\ (w^2)_{j-1/2}^n+P_3^n\ (gt)_{j-1/2}^n$$
$$-\alpha_n(u_{j-1/2}^{n-1}w_{j-1/2}^n-w_{j-1/2}^{n-1}u_{j-1/2}^n-(ft)_{j-1/2}^n$$
$$-t_{j-1/2}^{n-1}f_{j-1/2}^n+f_{j-1/2}^{n-1}t_{j-1/2}^n)=S_{j-1/2}^{n-1} \tag{29f}$$

where

$$T_{j-1/2}^{n-1}=\alpha_n[-(u^2)_{j-1/2}^{n-1}+(fv)_{j-1/2}^{n-1}]$$
$$-\{((bv)_j^{n-1}-(bv)_{j-1}^{n-1})/h_j+P_1^{n-1}(fv)_{j-1/2}^{n-1}$$
$$+P_2^{n-1}[1-(u^2)_{j-1/2}^{n-1}]+P_3^{n-1}(gv)_{j-1/2}^{n-1}\}-P_2^n \tag{30a}$$

$$S_{j-1/2}^{n-1}=\alpha_n[-(uw)_{j-1/2}^{n-1}+(ft)_{j-1/2}^{n-1}]$$
$$-\{((bt)_j^{n-1}-(bt)_{j-1}^{n-1})/h_j+P_1^{n-1}(ft)_{j-1/2}^{n-1}$$
$$+P_4^{n-1}[1-(uw)_{j-1/2}^{n-1}]+P_3^{n-1}[1-(w^2)_{j-1/2}^{n-1}]$$
$$+P_3^{n-1}(gt)_{j-1/2}^{n-1}\}-(P_3^n+P_4^n) \tag{30b}$$

$$\alpha_n=x_{n-1/2}/(x_n-x_{n-1}) \tag{30c}$$

The boundary conditions (25) yield at $x=x_n$

$$f_0^n=0,\ g_0^n=0,\ u_0^n=0,\ w_0^n=0,\ u_J^n=1,\ w_J^n=1 \tag{31}$$

We next consider the general equations (17) and (18) and again write them in terms of a first-order system of partial-differential equations. Again we get the same equations (26a-26d). Equations (26e) and (26f) are replaced by

$$(bv)'+P_1fv+P_2(1-u^2)+P_5(1-uw)$$
$$+P_6gv=x\left[u\frac{\partial u}{\partial x}-v\frac{\partial f}{\partial x}+P_7\left[w\frac{\partial u}{\partial z}-v\frac{\partial g}{\partial z}\right]\right] \tag{32a}$$

$$(bt)'+P_1ft+P_4(1-uw)+P_3(1-w^2)$$
$$+P_6gt=x\left[u\frac{\partial w}{\partial x}-t\frac{\partial f}{\partial x}+P_7\left[w\frac{\partial w}{\partial z}-t\frac{\partial g}{\partial z}\right]\right] \tag{32b}$$

where

$$P_7=(w_e/u_e) \tag{33}$$

We now consider the net cube shown in Fig. 2 and introduce the new net points

$$z_0=0, \quad z_i=z_{i-1}+r_i, \quad i=1,2,\ldots, I \tag{34}$$

in addition to the ones introduced in Eq. (27).

The difference equations which are to approximate Eq. (26) are obtained by averaging about the midpoint $(x_n, z_i, \eta_{j-1/2})$

$$(f_j^{n,i}-f_{j-1}^{n,i})/h_j=u_{j-1/2}^{n,i} \tag{35a}$$

$$(u_j^{n,i}-u_{j-1}^{n,i})/h_j=v_{j-1/2}^{n,i} \tag{35b}$$

$$(g_j^{n,i}-g_{j-1}^{n,i})/h_j=w_{j-1/2}^{n,i} \tag{35c}$$

where, for example,

$$u_{j-1/2}^{n,i}=\tfrac{1}{2}(u_j^{n,i}+u_{j-1}^{n,i})$$

The difference equations which are to approximate Eqs. (32a and b) are rather lengthy. To illustrate the difference

equations to equations similar to Eqs. (32a) and (32b), we consider the following model equation

$$v' + P_1 fv = x[u(\partial u/\partial x) + P_7 w(\partial u/\partial z)] \tag{36}$$

The difference equations for this equation are

$$(\bar{v}_h - \bar{v}_{j-1})/h_j + (P_1)^{n-1/2}_{i-1/2}(\overline{fv})_{j-1/2} = x^{n-1/2}\left[\bar{u}_{j-1/2}\left[\frac{\bar{u}_n - \bar{u}_{n-1}}{k_n}\right] + (P_7)^{n-1/2}_{i-1/2}\,\bar{w}_{j-1/2}\left[\frac{\bar{u}_i - \bar{u}_{i-1}}{r_i}\right]\right] \tag{37}$$

where, for example,

$$\bar{v}_j = \tfrac{1}{4}(v_j^{n,i} + v_j^{n,i-1} + v_j^{n-1,i-1} + v_j^{n-1,i})$$

$$\bar{u}_n = \tfrac{1}{4}(u_j^{n,i} + u_j^{n,i-1} + u_{j-1}^{n,i} + u_{j-1}^{n,i-1})$$

$$\bar{u}_i = \tfrac{1}{4}(u_j^{n,i} + u_j^{n-1,i} + u_{j-1}^{n,i} + u_{j-1}^{n-1,i})$$

$$(P_1)^{n-1/2}_{i-1/2} = \tfrac{1}{4}(P_i^n + P_{i-1}^n + P_i^{n-1} + P_{i-1}^{n-1})$$

the boundary conditions (25) yield at $x = x_n$, and at $z = z_i$

$$f_0^{n,i} = 0,\ g_0^{n,i} = 0,\ u_0^{n,i} = 0,\ w_0^{n,i} = 0,\ u_J^{n,i} = 1,\ w_J^{n,i} = 1 \tag{38}$$

Equations (29) for the attachment-line flow and Eqs. (35) and the difference equations for Eqs. (32) for the general case are imposed for $j = 1,2,\ldots J$. If we assume $(f_j^{n-1},\ u_j^{n-1},\ v_j^{n-1},\ g_j^{n-1},\ w_j^{n-1},\ t_j^{n-1})$ to be known for $0 \le j \le J$, then Eq. (29) for $1 \le j \le J$ and the boundary condition (31) yield an implicit nonlinear algebraic system of $6J+6$ equations in as many unknowns $(f_j^n,\ u_j^n,\ v_j^n,\ g_g^n,\ w_j^n,\ t_j^n)$. This system can be solved very effectively by using Newton's methods. For details, see Ref. 12.

Similarly, for the general case, if we assume

$$(f_j^{n-1,i-1},\ u_j^{n-1,i-1},\ v_j^{n-1,i-1},\ g_j^{n-1,i-1},\ w_j^{n-1,i-1},\ t_j^{n-1,i-1}),$$

$$(f_j^{n,i-1},\ u_j^{n,i-1},\ v_j^{n,i-1},\ g_j^{n,i-1},\ w_j^{n,i-1},\ t_j^{n,i-1})$$

and

$$(f_j^{n-1,i},\ u_j^{n-1,i},\ v_j^{n-1,i},\ g_j^{n-1,i},\ w_j^{n-1,i},\ t_j^{n-1,i})$$

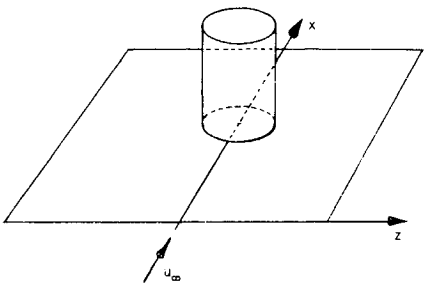

Fig. 3 Flow past a flat plate with attached cylinder.

to be known for $0 \le j \le J$, then the differenced equations for the general case can be solved by a similar procedure used by attachment-line flow equations.

VI. Results

The method discussed in the previous sections is applicable for both laminar and turbulent boundary layers. For laminar layers the study conducted in Ref. 9 shows that highly accurate solutions for two-dimensional flows can be obtained by taking 25 to 30 points across the boundary layer. In Sec. VIA, we present a similar study for three-dimensional laminar flows and compare out calculations with those reported in literature.

For turbulent flows, the accuracy of the results depends on the accuracy of the numerical method and on the accuracy of the model for the Reynolds stresses. According to the study conducted in Ref. 7, for semi-three dimensional turbulent boundary layers, accuracy of the eddy-viscosity formulation was found to be quite good; the calculated results agreed well with experiment and with those calculated by Bradshaw's method.[4] In Sec. VIB, we present a similar study for three-dimensional turbulent flows and compare our calculations with experimental data.

A. Laminar Flows

We consider a three-dimensional laminar flow past a flat plate with attached cylinder (Fig. 3). For this flow, the inviscid velocity distribution is given by

$$u_e = u_\infty[1 + a^2(\Delta_2/\Delta_1^2)] \tag{39a}$$

$$w_e = -2u_\infty a^2(\Delta_3/\Delta_1^2) \tag{39b}$$

Table 1 Comparison of calculated results with those of Ref. 15.[a]

	$z=0$				$z=3.05$			
	Ref. 15		Present Method		Ref. 15		Present method	
x	f''_w	ν	f''_w	ν	f''_w	ν	f''_w	ν
0	0.4696	...	0.4694	3	0.4696	...	0.4694	...
2.44	0.4655	3	0.4651	2	0.4656	1	0.4652	2
4.88	0.4598	3	0.4596	2	0.4602	1	0.4598	2
7.32	0.4524	4	0.4523	2	0.4530	1	0.4528	2
9.76	0.4426	4	0.4426	2	0.4436	2	0.4435	2
12.20	0.4292	4	0.4294	2	0.4310	2	0.4309	2
14.64	0.4106	4	0.4111	3	0.4136	3	0.4136	2
17.08	0.3839	4	0.3849	3	0.3890	3	0.3890	2
	$z=6.01$				$z=8.54$			
	Ref. 15		Present method		Ref. 15		Present method	
x	f''_w	ν	f''_w	ν	f''_w	ν	f''_w	ν
0	0.4696	..	0.4694	...	0.4696	...	0.4694	...
2.44	0.4660	1	0.4656	2	0.4664	1	0.4659	2
4.88	0.4611	1	0.4606	2	0.4621	1	0.4616	2
7.32	0.4548	2	0.4544	2	0.4568	2	0.4563	2
9.76	0.4467	2	0.4463	2	0.4502	2	0.4499	2
12.20	0.4361	3	0.4359	2	0.4419	3	0.4417	2
14.64	0.4221	3	0.4222	2	0.4314	3	0.4313	2
17.08	0.4032	4	0.4035	2	0.4182	4	0.4184	2

[a] $\eta_\infty = 8$, $\Delta\eta = 0.28$, $\Delta z = 0.61$, $\Delta x = 0.61$. ν denotes the iteration number.

Table 2 Effect of x-spacing on the results[a]

	$z=0$						$z=4.88$					
x	$f''_w(\Delta x/4)$	ν	$f''_w(\Delta x/2)$	ν	$f''_w(\Delta x)$	ν	$f''_w(\Delta x/4)$	ν	$f''_w(\Delta x/2)$	ν	$f''_w(\Delta x)$	ν
4.88	0.32489	2	0.32486	3	0.32475	3	0.32524	2	0.32518	2	0.324813	2
9.76	0.31298	3	0.31295	3	0.31283	3	0.31430	2	0.31421	2	0.31387	2
14.64	0.29093	3	0.29087	3	0.29065	3	0.29492	2	0.29479	2	0.29426	2
19.52	0.24558	3	0.24548	3	0.24513	3	0.25805	3	0.25786	3	0.23708	2
24.40	0.13022	3	0.13059	4	0.13152	4	0.17875	3	0.17865	3	0.17782	3

[a] $\eta_\infty=8$, $\Delta\eta=0.4$, $\Delta z=4.88$, $\Delta x=4.88$.

where

$$\Delta_1=(x-x_0)^2+z^2 \tag{40a}$$

$$\Delta_2=-(x-x_0)^2+z^2 \tag{40b}$$

$$\Delta_3=(x-x_0)z \tag{40c}$$

Here u_∞ is a reference velocity, a is the cylinder radius, and x_0 denotes the distance of cylinder axis from the leading edge, $x=0$. This flow has been computed extensively and accurately by Sowerby,[13] Dwyer,[14] Fillo and Burbank,[15] so we employ it as a test case.

To make a direct comparison between our calculated results and with those obtained by Fillo and Burbank,[15] we have chosen $u_\infty=3050$ cm/sec, $a=6.1$ cm, $x_0=45.7$ cm, $\eta_\infty=8.0$, $\Delta\eta=0.28$, $\Delta x=\Delta z=0.61$. The results are shown in Table 1. The number of iterations ν and some of the results tabulated under Ref. 15 were provided to us by Professor Fillo. The f''_w-values obtained by Fillo and Burbank differ from our f''_w-values by a factor of $\sqrt{2}$ due to a different transformation used by them. For this reason, we have multiplied our f''_w-values by $\sqrt{2}$. To keep the computer cost down, we have limited x to 17.08 for the Δx-spacing considered in Table 1. As can be seen from the comparisons, our calculated results are in good agreement with those computed by Fillo and Burbank. In our calculations we noted that for all x-stations, the solutions converged quadratically and required no more than 3 iterations. Our convergence criterion for laminar flows was based on the requirement that the difference between two successive values of f''_w values be less than a specific number of γ which was taken as 10^{-4},

$$|(f''_w)^{\nu+1}-(f'')^{\nu}_w|=|\delta f''_w|\le 10^{-4} \tag{41}$$

Table 2 shows the effect of Δx-spacing on the calculated f''_w-values for a fixed Δz and $\Delta\eta$-spacings. Here we have taken $\eta_\infty=8$, $\Delta\eta=0.4$, $\Delta z=4.88$, and used the three sets of x-spacings: Δx, $\Delta x/2$, $\Delta x/4$, with Δx equal to 4.88.

Table 3 shows the effect of Δz-spacing on the calculated f''_w-values for a fixed Δx and $\Delta\eta$-spacings. Here we have taken $\eta_\infty=8$, $\Delta\eta=0.4$, $\Delta x=4.88$, and used Δz, $\Delta z/2$, $\Delta z/4$ in $z=0$ and $z=4.88$

Tables 4 and 5 show the effect of $\Delta\eta$-spacing on the calculated f''_w and g''_w values, respectively, for a fixed Δx and Δz-spacings, namely, $\Delta x=4.88$, $\Delta z=4.88$, with $\eta_\infty=8$. The η_∞-spacings were: 1.6, 0.80, and 0.40, corresponding to 6, 11, and 21 points across the boundary layer. Table 4 also shows the Richardson extrapolated f''_w $(\Delta\eta/2, \Delta\eta)$ values obtained from

$$f''_w\left(\frac{\Delta\eta}{2},\Delta\eta\right)=\frac{(\Delta\eta/2)^2 f''_w(\Delta\eta)-(\Delta\eta)^2 f''_w(\Delta\eta/2)}{(\Delta\eta/2)^2-(\Delta\eta)^2} \tag{42a}$$

and the f''_w $(\Delta\eta/4, \Delta\eta/2, \Delta\eta)$ values obtained from

$$f''_w\left(\frac{\Delta\eta}{4},\frac{\Delta\eta}{2},\Delta\eta\right)$$
$$\frac{(\Delta\eta/4)^2 f''_w(\Delta\eta/2,\Delta\eta)-(\Delta\eta)^2 f''_w(\Delta\eta/4,\Delta\eta/2)}{(\Delta\eta/4)^2-(\Delta\eta)^2} \tag{42b}$$

Table 3 effect of z-spacing on the results.[a]

	$z=4.88$			
x	$f''_w(\Delta z/4)$	ν $f''_w(\Delta z/2)$	ν $f''_w(\Delta z)$	ν
4.88	0.32502	2 0.32527	2 0.324813	2
9.76	0.31324	2 0.31437	2 0.31387	2
14.64	0.29359	2 0.29522	2 0.29426	2
19.52	0.25772	2 0.25877	2 0.25708	2
24.40	0.18046	3 0.17836	3 0.17782	3

[a] $\eta_\infty=8$, $\Delta\eta=0.4$, $\Delta z=4.88$, $\Delta x=4.88$.

Table 4 Effect of $\Delta\eta$-spacing on the f''_w-values.[a]

	$z=0$								
x	$f''_w(\Delta\eta/4)$	ν	$f''_w(\Delta\eta/2)$	ν	$f''_w(\Delta\eta)$	ν	$f''_w(\Delta\eta/2,\Delta\eta)$	$f''_w(\Delta\eta/4,\Delta\eta/2)$	$f''_w(\Delta\eta/4\cdot\Delta\eta/2,\Delta\eta\sqrt{\ })$
0	0.331771	3	0.330853	3	0.326696	3	0.332239	0.332077	0.332066
4.88	0.324747	3	0.324089	3	0.320799	3	0.325186	0.324966	0.324951
9.76	0.312826	3	0.312766	3	0.311389	3	0.313225	0.312846	0.312821
14.64	0.290646	3	0.291886	3	0.294632	3	0.290971	0.290233	0.290184
19.52	0.245131	3	0.249604	3	0.262254	3	0.245387	0.243640	0.243524
24.40	0.131523	4	0.146914	4	0.189551	3	0.132702	0.126393	0.125972
	$z=4.88$								
x	$f''_w(\Delta\eta/4)$	ν	$f''_w(\Delta\eta/2)$	ν	$f''_w(\Delta\eta)$	ν	$f''_w(\Delta\eta/2,\Delta\eta)$	$f''_w(\Delta\eta/4,\Delta\eta/2)$	$f''_w(\Delta\eta/4,\Delta\eta/2,\Delta\eta)$
0	0.331771	...	0.330853	...	0.326696	...	0.332239	0.332077	0.332066
4.88	0.324813	2	0.323686	2	0.31893	2	0.325271	0.325189	0.325184
9.76	0.313870	2	0.312232	2	0.30599	2	0.314313	0.314416	0.314423
14.64	0.294259	2	0.291435	2	0.281645	3	0.294698	0.295200	0.295233
19.52	0.257077	2	0.251575	2	0.233778	3	0.257507	0.258911	0.259005
24.40	0.177822	3	0.166049	3	0.129445	3	0.178250	0.181746	0.181979

[a] $\eta_\infty=8$, $\Delta x=4.88$, $\Delta z=4.88$, $\Delta\eta=1.6$.

Table 5 Effect of $\Delta\eta$-spacing on the g''_w-values.[a]

			$z=0$			
x	$g''_w(\Delta\eta/4)$	$\nu\, g''_w(\Delta\eta/2)$	$\nu\, g''_w(\Delta\eta)$	$\nu\, g''_w(\Delta\eta/2,\Delta\eta)$	$g''_w(\Delta\eta/4,\Delta\eta/2)$	$g''_w(\Delta\eta/4,\Delta\eta/2,\Delta\eta)$
0	0.331771	3 0.330853	3 0.326696	3 0.332239	0.332077	0.332066
4.88	0.699355	3 0.689942	3 0.652078	3 0.702563	0.702493	0.702488
9.76	1.11659	3 1.09371	3 1.00576	3 1.12303	1.12422	1.12430
14.64	1.60938	3 1.56562	3 1.40315	3 1.61978	1.62397	1.62425
19.52	2.22412	3 2.14633	3 1.86621	3 2.23970	2.25005	2.25074
24.40	3.07845	4 2.93784	4 2.44324	3 3.10271	3.12532	3.12683
			$z=4.88$			
x	$g''_w(\Delta\eta/4)$	$\nu\, g''_w(\Delta\eta/2)$	$\nu\, g''_w(\Delta\eta)$	$\nu\ g''_w(\Delta\eta/2,\Delta\eta)$	$g''_w(\Delta\eta/4,\Delta\eta/2)$	$g''_w(\Delta\eta/4,\Delta\eta/2,\Delta\eta)$
0	0.331771	− 0.330854	... 0.326696	... 0.33224	0.332077	0.332066
4.88	0.718849	2 0.722325	2 0.732139	2 0.719054	0.717690	0.717599
9.76	1.12440	2 1.12488	2 1.12565	2 1.12462	1.12424	1.12421
14.64	1.60331	2 1.59606	2 1.57555	3 1.60290	1.60573	1.60592
19.52	2.18005	2 2.14742	2 2.06185	3 2.17594	2.19093	2.19193
24.40	2.92266	3 2.82403	3 2.60111	3 2.89834	2.95554	2.95935

[a] $\eta_\infty=8$, $\Delta x=4.88$, $\Delta z=4.88$, $\Delta\eta=1.6$.

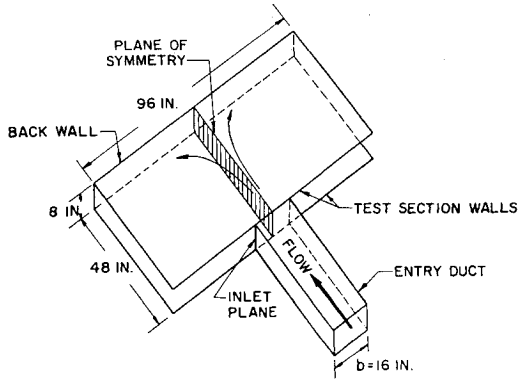

Fig. 4 Schematic drawing of Johnston's test geometry.

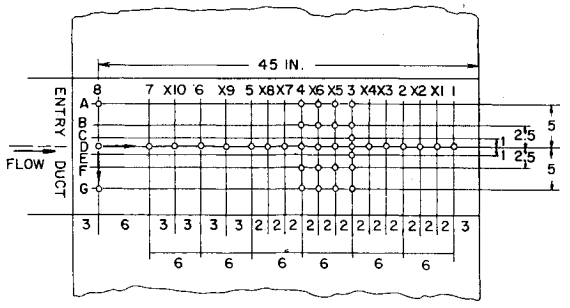

Fig. 5 Sketch showing the measured stations.

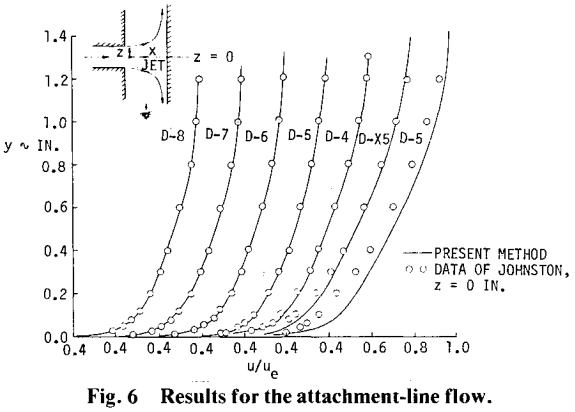

Fig. 6 Results for the attachment-line flow.

B. Turbulent Flows

Because of the nature of a turbulent boundary layer, it is necessary to use a variable grid across the boundary layer. Although a number of variable-grid systems can be used with the present method, here, as in our previous studies, we use a net given by

$$\eta_j=h(k^j-1)/(k-1) \quad j=1,2,\ldots J. \tag{43}$$

In Eqs. (43) there are 2 parameters: h_1, the length of the first $\Delta\eta$-step, and K, the ratio of two successive steps, $K=h_j/h_{j-1}$. The total number of points across the layer can be calculated by the following formula

$$J=\frac{ln[1+(K-1)\eta_\infty/h_1]}{ln\,K} \tag{44}$$

In our calculations we select h_1 and K and calculate the η_∞. Several studies conducted with this present method showed that approximately 20-30 points are sufficient for turbulent flows. For this reason, the turbulent-flow calculations in the present study were obtained with 30 or less η-points.

To check the accuracy of the method for three-dimensional turbulent boundary layers, we have considered two sets of experimental data: they are due to Johnston[16] and East and Hoxey.[17] Other comparisons with experiment are being made currently and will be reported later.

1. Data of Johnston

Johnston's experimental apparatus consisted of a rectangular inlet duct from which an issuing jet impinged on an end wall 48 in. from the outlet of the channel. The jet was confined on the top and bottom by flat surfaces, and the boundary layer which developed on the floor of the test section was probed. Figure 4 shows the schematic drawing of Johnston's test geometry, and Fig. 5 shows the locations where the measurements were conducted.

The inviscid external velocity distribution for this test can be obtained by the following formulas given in Milne-Thompson.[18]

$$F=-\pi\left[0.75\left(\frac{x}{b}\right)-x_0\right]-ln\left[\frac{((1-u_e^2-w_e^2)^2+4w_e^2)^{1/2}}{(1-u_e)^2+w_e^2}\right]$$

$$-\tan^{-1}\left[\frac{2u_e}{1-u_e^2-w_e^2}\right]=0 \tag{45a}$$

$$G=-0.75\pi\left(\frac{z}{b}\right)+ln\left[\frac{((1-u_e^2-w_e^2)^2+4u_e^2)^{1/2}}{(1-w_e)^2+u_e^2}\right]$$

$$+\tan^{-1}\left[\frac{2w_e}{1-u_e^2-w_e^2}\right]=0 \tag{45b}$$

where $x_0=45/16$ and $b=16$.

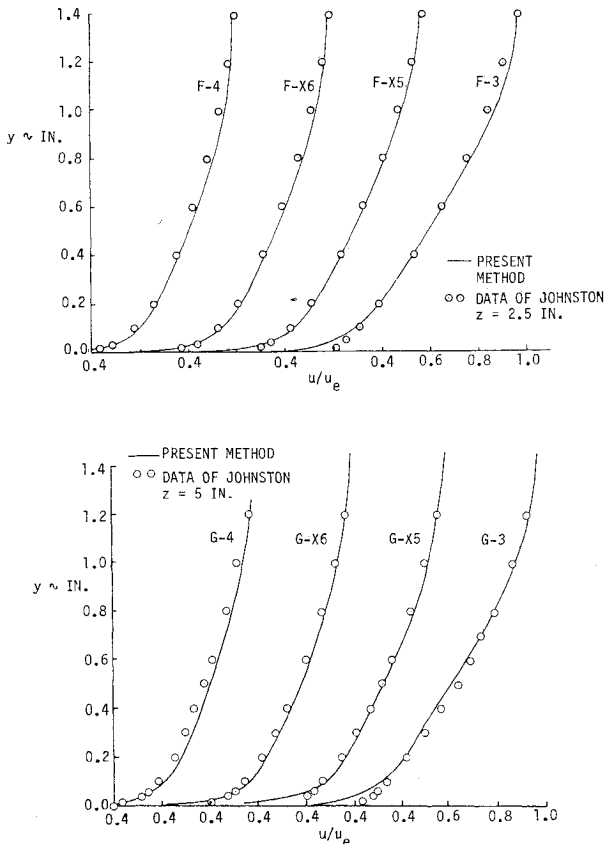

Fig. 7 Results for the flow off the line of symmetry.

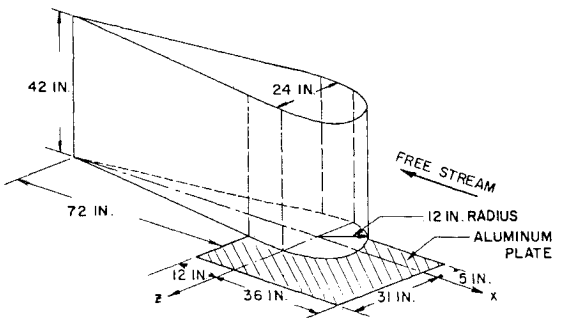

Fig. 8 Schematic drawing of East and Hoxey's test setup.

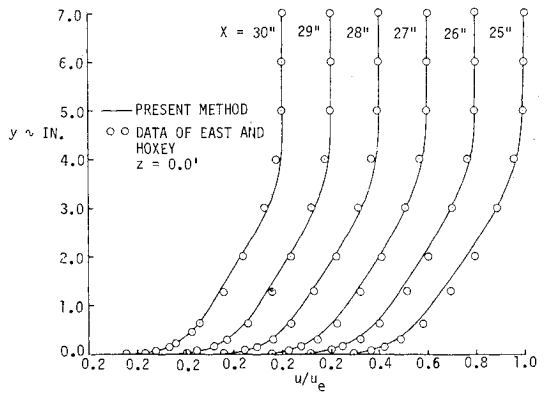

Fig. 9 Results for the attachment-line flow.

In the present method, the solution begins on the attachment line at $x=0$, $z=0$, and proceeds downstream. At station $x=0$, $z=0$, the flow is laminar, and it becomes turbulent at any specified station where $x>0$, $z>0$. The calculations can be started at any x-location by inputting the initial velocity profiles. Reference 19 describes such a procedure. For the data of Johnston, we have started the

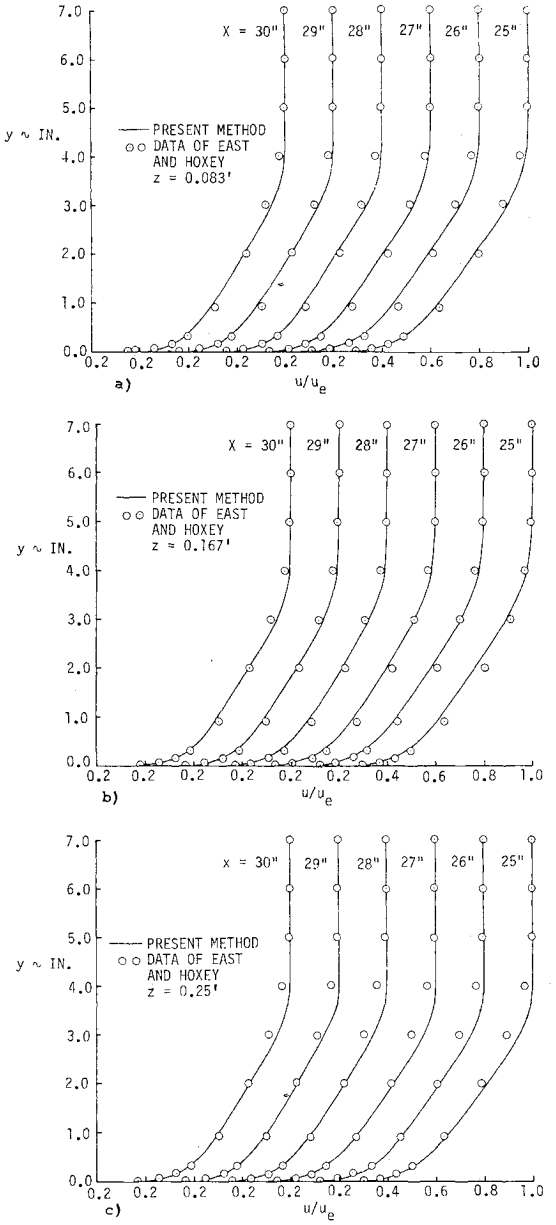

Fig. 10 Comparison of calculated external velocity distribution and measured velocity distribution on $z=0$.

calculations at $x=0$, $z=0$, and matched the initial experimental velocity profile as closely as possible.

Figure 6 shows the results for the attachment-line flow. These calculations were made by using $h_1=0.05$, $K=1.226$ and starting the calculations at $x=0$, $z=0$, with $\eta_\infty=20$. With this selection of h_1, K, and η_∞, we initially had 23 points across the boundary layer. The flow was laminar and was made turbulent at $x=0.1$ by activating the eddy-viscosity formulas. With this procedure, we matched the first experimental velocity profile, D-8 at $x=6$, by using a total of four x-stations although we used 26 x-stations to do the calculations up to D-3. At the last x-station η_∞ was 54 with 28 η-points across the boundary layer. The last profile in that figure is close to the station where the flow separation was observed. This may be the reason for poor agreement between the calculated and experimental profiles.

Figure 7 shows the velocity profiles off the line of symmetry. The calculations were made by taking $z=1,2.5$, and 5 in. As in the attachment-line flow, the agreement with experiment is satisfactory.

2. Data of East and Hoxey

The data of East and Hoxey consists of a flow formed by placing an obstruction in a thick two-dimensional boundary

layer. The strong pressure gradients imposed by the obstruction, Fig. 8 caused the boundary layer to become three-dimensional and to separate. The measurements were made in the three-dimensional boundary layer upstream of and including the three-dimensional separation.

Figure 9 shows the calculated velocity profiles for the attachment-line flow. These calculations were made by inputting the initial velocity profile at $x=6.5$ ft, which corresponded to $x=30$ in. in the experimental data. The velocity distribution was obtained by using Eq. (39) with $a=12$ in.

Figure 10 shows the velocity profiles off the line of symmetry. These calculations were made by using the experimental velocity distribution. In general the agreement with experiment is satisfactory.

In conclusion, the method presented here for predicting the full three-dimensional laminar and turbulent boundary layers in Cartesian coordinates is found to be in good agreement with other numerical solutions and with available experimental data.

References

[1] Hunt, J. L., Bushnell, D. M., and Beckwith, I. E., "Finite-Difference Analysis of the Compressible Turbulent Boundary Layer on a Blunt Swept Slab With Leading-Edge Blowing," *Analytical Methods in Aircraft Aerodynamics*, Paper 19, NASA SP-228, Symposium held at NASA Ames Research Center, Moffett Field, Calif., Oct. 1969, pp. 417-472, see also TN D-6203, March 1971, NASA.

[2] Bushnell, D. M. and Beckwith, I. E., "Calculation of Nonequilibrium Hypersonic Turbulent Boundary Layers and Comparisons with Experimental Data," *AIAA Journal*, Vol. 8, p. 1462, 1970.

[3] Adams, J. C., "Three-Dimensional Compressible Turbulent Boundary Layer on a Sharp Cone at Incidence in Supersonic Flow," *International Journal of Heat and Mass Transfer*, Vol. 17, June 1974, pp. 581-593.

[4] Bradshaw, P., "Calculation of Three-Dimensional Turbulent Boundary Layers," *Journal of Fluid Mechanics*, Vol. 46, pt. 3, April 1971, pp. 417-445.

[5] Nash, J. F., "The Calculation of Three-Dimensional Turbulent Boundary Layers In Incompressible Flow," *Journal of Fluid Mechanics*, Vol. 37, July 1969, pp. 625-642.

[6] Harris, J. E. and Morris, D. J., "Solution of the Three-Dimensional Compressible Laminar and Turbulent Boundary-Layer Equations with Comparisons to Experimental Data," presented at the 4th International Conference on Numerical Methods in Fluid Dynamics, Boulder, Colo., June 1974.

[7] Cebeci, T., "Calculation of Three-Dimensional Boundary Layers, I. Swept Infinite Cylinders and Small Cross Flow," *AIAA Journal*, Vol. 12, June 1974, pp. 779-786.

[8] Keller, H. B., *A New Difference Scheme for Parabolic Problems in "Numerical Solution of Partial Differential Equations,"* edited by J. Bramble, Vol. II, Academic Press, New York, 1970.

[9] Keller, H. B. and Cebeci, T., "Accurate Numerical Methods for Boundary Layers, I. Two-Dimensional Laminar Flows," *Proceedings of the Second International Conference on Numerical Methods in Fluid Dynamics*, Lecture Notes in Physics, Springer-Verlag, New York, Vol. 8, 1971.

[10] Keller, H. B. and Cebeci, T., "Accurate Numerical Methods for Boundary Layers, II. Two-Dimensional Turbulent Flows," *AIAA Journal*, Vol. 10, Sept. 1972, pp. 1197-1200.

[11] Cebeci, T. and Smith, A.M.O., *Analysis of Turbulent Boundary Layers*, Academic Press, New York, 1974.

[12] Isaacson, E. and Keller, H. B., *Analysis of Numerical Methods*, Wiley, New York, 1966.

[13] Sowerby, L., "The Three-Dimensional Laminar Layer on a Flat Plate," *Journal of Fluid Mechanics*, Vol. 22, Pt. 3, 1965, pp. 587-598.

[14] Dwyer, H. A., "Solution of a Three-Dimensional Boundary-Layer Flow with Separation," *AIAA Journal*, Vol. 6, July 1968, pp. 1336-1342.

[15] Fillo, J. A. and Burbank, R., "Calculation of Three-Dimensional Laminar Boundary-Layer Flows," *AIAA Journal*, Vol. 10, March 1972, pp. 353-355.

[16] Johnston, J. P., Three-Dimensional Turbulent Boundary Layer, Rept. 39, May 1957, M.I.T. Gas Turbine Lab., Cambridge, Mass.

[17] East, L. F. and Hoxey, R. P., "Low-Speed Three-Dimensional Turbulent Boundary-Layer Data," Pt. I, TR 69041, March 1969, Royal Aircraft Establishment, Farnborough, England.

[18] Milne-Thompson, L. M., *Theoretical Hydrodynamics*, MacMillan, New York, 1960.

[19] Cebeci, T., Mosinskis, G. J., and Kaups, K., "A General Method for Calculating Three-Dimensional Incompressible Laminar and Turbulent Boundary Layers. I. Swept Infinite Cylinders and Small Cross Flow," Rept. MDC J5694, 1972, McDonnell Douglas Corp., Long Beach, Calif.